Wavefunctions, expectation values and scars on Poincaré sections - A scattering approach

Article *in* Journal of Physics A General Physics · January 1999

DOI: 10.1088/0305-4470/29/12/026

J. Phys. A: Math. Gen. **29** (1996) 3213–3231. Printed in the UK

Wavefunctions, expectation values and scars on Poincaré sections—a scattering approach

D Klakow and U Smilansky

Department of Physics of Complex Systems, The Weizmann Institute of Science, Rehovot 76 100, Israel

Received 24 November 1995, in final form 22 February 1996

Abstract. Using the scattering approach to quantization, we define an appropriate representation of the billiard wavefunction on the scattering Poincaré section. The expectation values of smooth operators in terms of these Poincaré section wavefunctions are expressed as sums over periodic orbits. A special operator is used to define scars on the section and the relation to scars in configuration space is discussed and demonstrated numerically.

1. Introduction

The structure of the eigenstates of a quantum system which is chaotic in the classical limit has been a major issue in quantum chaology. The Shnirelman theorem [1] states that as the energy goes to infinity, the probability density of most eigenstates of a chaotic billiard approaches a uniform distribution. Thus, the discovery of regions of high probability along classical periodic orbits came as a surprise. These structures, called 'scars', were first observed by McDonald and Kaufman [2] and later also by Heller [3] for the stadium billiard. Bogomolny [4] developed the semiclassical theory of scars for wavefunctions, and a similar analysis in phase-space, using Wigner functions, was performed by Berry [5]. Significant progress was achieved by Agam and Fishman [6] who were able to derive a semiclassical Wigner function without having to resort to energy smearing as previous authors did, and hence provided a much clearer description. To achieve this, they extended the method of Berry and Keating [7] for deriving a semiclassical expression for the spectral determinant as a finite sum over 'composite orbits'. This theory gave them for the first time the means to predict whether a given wavefunction should be scarred by a particular orbit [8].

One of the most convenient tools in the analysis of classical Hamiltonian dynamics is the Poincaré section, which is used to convert the continuous time evolution into a discrete mapping. The main advantage in this construction is the reduction of the dimension of the effective phase space. The quantum mechanical treatment of the corresponding systems was traditionally carried out in the full configuration space, and only recently was quantization in terms of Poincaré sections introduced [9–15]. These studies focus mainly on the calculation of energy spectra, and the semiclassical versions of these methods make use of classical periodic orbits of the Poincaré map. In the present paper we would like to make one further step and construct the appropriate representation of the complete wavefunction on the section. In terms of these wavefunctions, we shall compute the semiclassical expression for expectation values of observables on the section. Since one of the main motivations of the present work is to identify scars on the section, we shall define an operator whose

0305-4470/96/123213+19$19.50

expectation value yields the properly smoothed probability density. It is not clear whether the occurrence of scars in configuration space implies a scarred section, and vice versa. However, if scars exist on the section, they should be easily observed as local maxima of these probability distributions. Scars were traditionally defined as enhanced probabilities along periodic orbits in phase space (for Wigner distributions) or in configuration space (for wavefunctions) [3, 5, 6, 9, 16, 17]. Searching for them on the Poincaré section can bring some practical advantage, since the high probability domains are expected to concentrate on points rather than on lines, so they might be easier to observe.

In order to investigate scars on the section, we first have to identify the quantum object which corresponds to a wavefunction on the section. We shall show that it is not necessarily the restriction of the wavefunction to the section! Consider, for example, the case of billiards. The section wavefunction is neither the normal derivative (for Dirichlet boundary conditions), nor the value of the wavefunction (for Neumann boundary conditions) at the boundary. This is somewhat counterintuitive, since for billiards, the interior wavefunctions can be expressed uniquely in terms of the normal derivative (or the wavefunction) along the boundary. One would expect therefore that these boundary functions, which store all the information about the interior wavefunction, will be the appropriate section wavefunctions. However, they are not. This simple example illustrates the need to define the appropriate representation of the wavefunction on the section and this is one of the main purposes of the present work. Some representations of section wavefunctions will be given at the end of section 3.3.

We shall formulate our theory within the scattering approach to quantization. In section 2 we shall briefly review this method, and introduce the necessary background and definitions. At this point we shall define the quantum Hilbert space which is the analogue of the classical phase space of the section. We shall then discuss the class of observables whose expectation values we are about to calculate, and in particular, define the scar observables. We shall express the expectation values of the observables in terms of the derivatives of a generalized ζ function, which will be the starting point of a semiclassical calculation. A semiclassical analysis and numerical illustrations of the main building blocks of the theory applied to the Limacon billiard will follow in the third section. We shall discuss and summarize our findings in the last section.

2. Expectation values on the section

2.1. The semiclassical secular equation

Before we come to our main topic, we would like to recall a common feature of all the semiclassical quantization schemes which are based on the dynamics on a Poincaré section: one defines a unitary operator $S(E)$ and the quantization condition is expressed via a secular function

$$\zeta(E) = \det(I - S(E)) \,. \tag{1}$$

The spectrum $\{E_t,\ t = 1, 2, \ldots\}$ is obtained as the zeros of the secular equation. At these energies, the S-matrix has an eigenvalue 1, and the corresponding eigenvector will be denoted by $|1_t\rangle$. In all cases, $S(E)$ is semiclassically unitary, and in the semiclassical limit it is represented by a matrix with a finite dimension Λ. As an example, consider the scattering approach to quantization. It was originally proposed for the quantization of billiards [10, 11, 13, 18, 20], and was recently extended to more general Hamiltonian systems [14]. In this method $S(E)$ is the restriction of the scattering matrix at an energy E,

to the semiclassically relevant space of non-evanescent modes. In Bogomolny's treatment [9], the $T(E)$ operator plays the same role. Since we will be mainly concerned with billiards, we use the wave number k and define the spectrum of wave numbers $\{k_t\}$ by $E_t = \hbar^2 k_t^2/2m$.

The connection to the classical dynamics comes through the identification of the S operator as the quantum counterpart of the Poincaré mapping on an appropriate section. We shall denote the classical action-angle variables on the section by (l, θ). For billiards, when the boundary is considered as an obstacle for scattering from the exterior, the S-matrix is analogous to the Poincaré scattering mapping [19, 23]. This, in turn, is isomorphic to the mapping which describes the interior dynamics on the section defined by the boundary [11, 18]. One of the consequences of the semiclassical correspondence between the S-matrix and the Poincaré mapping is that Λ is expressed as the phase-space area of the section, measured in units of $2\pi\hbar$. If, for example, the S-matrix describes the scattering from the exterior of a billiard, $\Lambda(k) = [k\Gamma/\pi]$ where $[\cdot]$ stands for the integer part, and Γ is the circumference of the billiard.

The semiclassical version of the secular equation (1) is derived in the following way. The determinant $\det(I - S)$ can be expressed as a function of all $\operatorname{Tr} S^n$, with $n \leqslant \Lambda$. Because of the semiclassical unitarity of S, it suffices to know only $\operatorname{Tr} S^n$ for $n \in \{1, \Lambda/2\}$ and the total scattering phase, $\mathrm{e}^{-\mathrm{i}\Theta} = \det S$. The semiclassical evaluation of these quantities provides the building blocks for the semiclassical ζ function. To the leading semiclassical order, $\Theta(E)$ is proportional to the smooth spectral counting function $\bar{N}(E)$,

$$\Theta(E) \approx 2\pi \bar{N}(E)\,. \tag{2}$$

Also,

$$\operatorname{Tr} S^n(k) \approx \sum_{p \in P_n} \frac{n_p}{|\mathrm{Det}(1 - M_p^{r_p})|^{1/2}}\, \mathrm{e}^{\mathrm{i}r_p(l_p k - \nu_p \pi/2)}\,. \tag{3}$$

Here, P_n is the set of all periodic orbits which are obtained by repeating r_p times the primitive orbits with periods n_p, such that $n_p r_p = n$. The length of the primitive orbit is l_p and ν_p is the Maslov index. M_p is the monodromy matrix of the primitive orbit (which only for billiard systems is independent of k). Thus, periodic orbits with only up to $\Lambda/2$ reflections have to be determined. The advantage of this approach is that the semiclassical approximation of the secular equation is written directly in a 'Riemann Siegel look-alike' form of the ζ function [7].

2.2. Quantum mechanics on the Poincaré section

The semiclassical correspondence between the S-matrix and the Poincaré map indicates that the Hilbert space, which is the quantum analogue of the section phase-space, is the Λ-dimensional space where the S matrix acts. We shall define the representation of the total scattering eigenfunction on the Poincaré section in the following way.

On the section, the position operator $\hat{\theta}$ has eigenvectors $\langle\theta|$. Thus, the object for inspection is $\langle\theta|1_t\rangle$ which is the wavefunction in the θ representation on the section. In order to clarify the relation between $\langle\theta|1_t\rangle$ and the full wavefunction, we have to invoke the basic concept of 'transparency' which is a basic element of the scattering approach [11, 23]. Any scattering state behaves asymptotically like

$$\Psi_l(\boldsymbol{r}) \to I_l(\boldsymbol{r}) + \sum_{l'} S_{l,l'}\, O_{l'}(\boldsymbol{r}) \qquad \text{as} \quad r \to \infty \tag{4}$$

where $I_l(\boldsymbol{r})$ and $O_l(\boldsymbol{r})$ are the asymptotic incoming and outgoing scattering wavefunctions. When the S-matrix has an eigenvalue 1, the linear combination of $\Psi_l(\boldsymbol{r})$ with coefficients

which are the corresponding eigenvector of S, can be extended to the interior as a proper interior wavefunction. (A rigorous description of the concept is given in [20, 21].) In this sense, the information contained in the eigenvector of the S-matrix suffices to construct both the section and the configuration space wavefunction.

We shall study observables A on the section. They can be represented by $\Lambda \times \Lambda$ Hermitian matrices. We shall assume A to be smooth on the quantum scale in a sense which is defined below. We shall show that $A_t \equiv \langle 1_t|A|1_t\rangle$ can be expressed semiclassically in terms of periodic orbits on the Poincaré section. This semiclassical expression will add another intuitive explanation of the role of $\langle\theta|1_t\rangle$ as the representation of the complete wavefunction on the section.

We shall start with some formal manipulations whose purpose will become clear later. They will enable us to cast the formalism in terms of a characteristic polynomial of some operator. The expectation values which we seek will be then expressed as a ratio of partial derivatives of this characteristic polynomial [22]. Consider two $\Lambda \times \Lambda$ matrices S and A, S is unitary with (a non-degenerate) spectrum $\mathrm{e}^{-\mathrm{i}\omega_l}$ on the unit circle, and A is Hermitian. We are looking for the expectation value of A, in a particular eigenstate $|r\rangle$ of S,

$$A_r = \langle r|A|r\rangle\,. \tag{5}$$

We now define the characteristic polynomial of the product $\mathrm{e}^{\alpha A}S$, where α is an arbitrary real variable:

$$g^+(\alpha,\omega) = \det(I - \mathrm{e}^{\mathrm{i}\omega}\,\mathrm{e}^{\alpha A}S)\,. \tag{6}$$

This is a polynomial in $\mathrm{e}^{\mathrm{i}\omega}$. It is useful to define the function

$$g^-(\alpha,\omega) = \det(I - \mathrm{e}^{-\mathrm{i}\omega}S^\dagger\,\mathrm{e}^{-\alpha A})\,. \tag{7}$$

The functions g^+ and g^- are related, and this calls for the introduction of a function $g(\alpha,\omega)$ through the relation,

$$g(\alpha,\omega) \equiv \mathrm{e}^{\mathrm{i}(\Theta-\omega\Lambda)/2}\,\mathrm{e}^{-\alpha\bar{A}/2}g^+(\alpha,\omega) = \mathrm{e}^{-\mathrm{i}(\Theta-\omega\Lambda)/2}\,\mathrm{e}^{\alpha\bar{A}/2}g^-(\alpha,\omega)\,. \tag{8}$$

Here we defined $\bar{A} = \operatorname{tr} A$. One can easily check that A_r can be expressed as the residue at $\omega = \omega_r$, of the logarithmic derivative of $g^+(\alpha,\omega)$ calculated at $\alpha = 0$. This follows from the identity

$$\frac{\partial}{\partial\alpha}\log g^+(\alpha,\omega)\bigg|_{\alpha=0} = \sum_l \frac{A_l}{1-\mathrm{e}^{-\mathrm{i}(\omega-\omega_l)}}\,. \tag{9}$$

Hence,

$$A_r = \mathrm{i}\left[\left(\frac{\partial g^+}{\partial\alpha}\right)\Big/\left(\frac{\partial g^+}{\partial\omega}\right)\right]_{\alpha=0,\omega=\omega_r} = \mathrm{i}\left[\left(\frac{\partial g}{\partial\alpha}\right)\Big/\left(\frac{\partial g}{\partial\omega}\right)\right]_{\alpha=0,\omega=\omega_r}\,. \tag{10}$$

The last equality follows simply from the definition of the function $g(\alpha,\omega)$ from (8).

Before proceeding with the semiclassical theory, we should explain what we mean by requiring the observables to be 'smooth on the quantum scale'. This requirement can be given a precise definition in the representation where the A operator is diagonal with eigenvalues a_q, $q = 1,\ldots,\Lambda$. In the semiclassical limit $\Lambda \gg 1$, and hence there exists an intermediate scale Δl with $\Lambda > \Delta l > 1$. We require that a_q be smooth on this scale. We shall also assume that the classical analogue of a_q is a well defined function $a(q)$ where (p,q) are phase-space variables on the section which are canonically conjugate to (l,θ). As an illustrative example, consider the operator which will be used to define scars on the sections

$$\langle\theta|A_{\mathrm{scar}}(\theta_0)|\theta'\rangle = \delta(\theta-\theta')f(\theta-\theta_0) \tag{11}$$

where $f(x)$ is a 2π-periodic and positive weight function with a width $2\pi/\Delta l$ and normalized to unity on the interval $[0, 2\pi]$. When $A_{\rm scar}(\theta_0)$ is applied to any function on the above interval, it yields its average value in the $2\pi/\Delta l$ vicinity of θ_0. In particular,

$$p_t(\theta_0) = \int_0^{2\pi}\int_0^{2\pi} \langle 1_t|\theta\rangle\langle\theta|A_{\rm scar}(\theta_0)|\theta'\rangle\langle\theta'|1_t\rangle \,{\rm d}\theta\,{\rm d}\theta' \tag{12}$$

yields the smooth distribution for the special eigenvector of $S(k_t)$ along the boundary. This is the function which should be scarred, if scars exist on the section. A different example for a smooth scar observable would be to define A as the projection on coherent states in the angular momentum representation. This yields a Husimi picture on the scattering section, which will be illustrated briefly in the third section.

2.3. Periodic orbit sum for expectation values on the section

We consider now the upper ω plane, and in order to calculate $g(\alpha, \omega)$ there, we use the definition of g in terms of g^+, equation (8), and expand $\log g^+(\alpha, \omega)$ with $S = S(k_t)$:

$$\log g^+(\alpha, \omega) = -\sum_{n=1}^{\infty} \frac{1}{n}\, {\rm e}^{{\rm i}\omega n}\, {\rm tr}({\rm e}^{\alpha A} S(k_t))^n \,. \tag{13}$$

We can always choose $\Im(\omega)$ to be sufficiently positive so that the expansion converges absolutely. We now introduce the semiclassical approximation to calculate ${\rm tr}({\rm e}^{\alpha A}S)^n$. We perform the calculation in the q representation where A is diagonal and smooth on the quantum scale. Next we substitute the semiclassical expression for the S-matrix in the q representation and perform the intermediate summations by the saddle-point approximation. Because of the requirement of smoothness, the presence of the A-dependent factors does not affect the saddle points, which are n-periodic points of the mapping induced by the classical analogue of the $S(k)$ operator. Using standard semiclassical manipulations, and assuming that the periodic points of the mapping are isolated, we obtain

$${\rm tr}({\rm e}^{\alpha A} S(k))^n \approx \sum_{p\in P_n} {\rm e}^{\alpha r_p \sum_{s=1}^{n_p} a(q_s)} \frac{n_p\, {\rm e}^{{\rm i}r_p(l_p k - \nu_p \pi/2)}}{|\det(I - M_p^{r_p})|^{1/2}} \tag{14}$$

which for $\alpha = 0$ is identical to (3). We shall introduce

$$a_p = \sum_{s=1}^{n_p} a(q_s) \tag{15}$$

which can be interpreted as the value of $a(q)$ accumulated along the p periodic orbit. As $n_p \to \infty$ the ratio a_p/n_p approaches the ergodic average of $a(q)$ which will be denoted by $\bar{a}$. Substituting (14) in (13) we can perform the sums over repetitions of primitive periodic orbits. The semiclassical approximation for g^+ reads

$$g^+_{\rm scl}(\alpha, \omega) = \prod_{m=0}^{\infty}\prod_{p} \left(1 - {\rm e}^{{\rm i}\omega n_p + \alpha a_p} t^+_{p,m}\right). \tag{16}$$

The second product runs through the primitive periodic orbits and

$$t^+_{p,m} = {\rm e}^{{\rm i}S_p - n_p\lambda_p(m+1/2)} \,. \tag{17}$$

For $\alpha = 0$ the product (16) over primitive periodic orbits converges in the absolute sense only if $\Im(\omega)$ is larger than the 'entropy barrier' which is given approximately by half the Lyapunov exponent λ. We are interested in the α dependence of g only in a narrow interval $|\alpha| < \alpha_c$. (As a matter of fact, since we need only the derivative of g at $\alpha = 0$, the width

of the interval is infinitesimal.) In this interval, the product will converge in the domain $\Im(\omega) > B = \lambda/2 + \alpha_c|\bar{a}|$.

The semiclassical expansion of g in the domain $\Im(\omega) < 0$ makes use of the definition of g in terms of g^- (8). Following similar steps one gets for the function g^-

$$g^-_{\rm scl}(\alpha,\omega) = \prod_{m=0}^{\infty}\prod_{p}\left(1 - \mathrm{e}^{-\mathrm{i}\omega n_p - \alpha a_p} t^-_{p,m}\right) \tag{18}$$

with

$$t^-_{p,m} = \mathrm{e}^{-\mathrm{i}S_p - n_p\lambda_p(m+1/2)}\,. \tag{19}$$

This product converges in the absolute sense only for $\Im(\omega) < -B$.

Using equation (8) we can define the semiclassical approximation for g as

$$g_{\rm scl} = \begin{cases} \mathrm{e}^{-\mathrm{i}(\Lambda\omega-\Theta)/2-\alpha\bar{A}/2} g^+_{\rm scl} & \Im(\omega) > B \\ \mathrm{e}^{+\mathrm{i}(\Lambda\omega-\Theta)/2+\alpha\bar{A}/2} g^-_{\rm scl} & \Im(\omega) < -B\,. \end{cases}$$

We now make the crucial assumption that $g_{\rm scl}$ preserves the analyticity of the exact g function, so that it can be continued to the domain $|\Im(\omega)| < B$ by a Cauchy integral. To this end, it is necessary to express the products in (16) and (18) as power series in $\mathrm{e}^{\pm\mathrm{i}\omega}$

$$g^\pm_{\rm scl} = 1 + \sum_{n=1}^{\infty} G^\pm_n\,\mathrm{e}^{\pm\mathrm{i}n\omega}\,. \tag{20}$$

To understand the structure of the coefficients $G^\pm_n$, we consider all the groups of primitive periodic orbits whose periods including repetitions sum up to n: $\sum_j r_{p_j} n_{p_j} = n$. Such groups are called 'pseudo-orbits' [5, 7] or 'composite orbits' [10] with composite period n and are formally obtained from (16) and (18) using the Euler identity [6, 23]. One can define the corresponding composite action and composite Lyapunov exponent as

$$\Phi_c = k\sum_j r_{p_j} l_{p_j} \qquad \Lambda_c = \frac{1}{n}\sum_j r_{p_j} n_{p_j}\lambda_{p_j} \tag{21}$$

where c is used to enumerate the composite orbits. We shall denote the set of all composite orbits with the same composite period, n, by C_n. In terms of these composite objects, we get

$$G^\pm_n = (-1)^n \sum_{c\in C_n} \mathrm{e}^{\pm\mathrm{i}\Phi_c - n\Lambda_c/2}\,\mathrm{e}^{\mp\alpha a_c} \tag{22}$$

where we define the composite weight $a_c = \sum_j r_{p_j} a_{p_j}$ and assume that the symbol $\sum_{c\in C_n}$ also includes the combinatorial factors from the application of the Euler identity. Breaking up the infinite products by the Euler identity is allowed as long as ω is in the domains where the products converge absolutely. Taking the contour of integration along lines which are parallel to the real axis within the domains of convergence, we get for arbitrary real ω

$$\begin{aligned} g_{\rm scl}(\omega) = {} & \frac{1}{2\pi\mathrm{i}}\int_{-\infty-\mathrm{i}\eta}^{\infty-\mathrm{i}\eta} \frac{\mathrm{d}\omega'}{\omega'-\omega}\,\mathrm{e}^{\mathrm{i}(\Lambda\omega'-\Theta)/2-\alpha\bar{A}/2}\sum_{n=0}^{\infty} G^-_n\mathrm{e}^{-\mathrm{i}n\omega'} \\ & + \frac{1}{2\pi i}\int_{\infty+\mathrm{i}\eta}^{-\infty+\mathrm{i}\eta} \frac{\mathrm{d}\omega'}{\omega'-\omega}\mathrm{e}^{-\mathrm{i}(\Lambda\omega'-\Theta)/2+\alpha\bar{A}/2}\sum_{n=0}^{\infty} G^+_n\mathrm{e}^{+\mathrm{i}n\omega'}\,. \end{aligned} \tag{23}$$

Here η is an arbitrary positive constant larger than B. The integral above can be carried out term by term, and only a few of them yield a non-vanishing contribution [23]. The resulting expression for $g_{\rm scl}$ is a finite polynomial in $\mathrm{e}^{\pm \mathrm{i}\omega}$ which, for odd Λ reads

$$g_{\rm scl} = \mathrm{e}^{-\mathrm{i}\Theta/2-\alpha\bar{A}/2}\sum_{n=0}^{[\Lambda/2]} G_n^- \,\mathrm{e}^{\mathrm{i}(\Lambda/2-n)\omega} + \mathrm{e}^{\mathrm{i}\Theta/2+\alpha\bar{A}/2}\sum_{n=0}^{[\Lambda/2]} G_n^+ \,\mathrm{e}^{-\mathrm{i}(\Lambda/2-n)\omega}\,. \quad (24)$$

For even Λ a term

$$\tfrac{1}{2}\,\mathrm{e}^{-\mathrm{i}\Theta/2-\alpha\bar{A}/2} G^-_{\Lambda/2} + \tfrac{1}{2}\,\mathrm{e}^{\mathrm{i}\Theta/2+\alpha\bar{A}/2} G^+_{\Lambda/2} \quad (25)$$

has to be added to the previous equation, which has to be treated separately because $G^{\pm}_{\Lambda/2}$ is its own symmetric partner. For all other n, $G^{\pm}_{\Lambda-n}$ and $G^{\mp}_n$ are related because of the unitarity of S and the structure of (6) and (7). A simple notation $\sum'$ can be introduced, which shall indicate that for even Λ the last term in the sum has to be multiplied by $\frac{1}{2}$. We can substitute the above expression for $g_{\rm scl}$ in (10) and obtain the expectation value A_t in terms of a finite expression which involves classical quantities exclusively,

$$A_t = \frac{\Im \sum_{n=0}^{'[\Lambda/2]} (-1)^n \sum_{c\in C_n} (\frac{\bar{A}}{/}2 - a_c)\,\mathrm{e}^{\mathrm{i}(\Phi_c+\Theta/2)}\,\mathrm{e}^{-n\Lambda_c/2}}{\Im \sum_{n=0}^{[\Lambda/2]} (-1)^n (\Lambda/2-n) \sum_{c\in C_n} \mathrm{e}^{\mathrm{i}(\Phi_c+\Theta/2)}\,\mathrm{e}^{-n\Lambda_c/2}}\,. \quad (26)$$

Note that at $k = k_t$ we have $\omega_r = 0 \bmod 2\pi$, since we are interested in the particular eigenvector of the S-matrix, whose eigenvalue is 1. Hence, for consistency, the eigenvalue E_t has to be taken from the semiclassical spectral determinant. A clearer expression follows after rearranging the terms and writing the above formula as

$$A_t = \frac{\bar{A} + A_t^{\rm osc}}{\Lambda + L_t^{\rm osc}} \quad (27)$$

where

$$A_t^{\rm osc} = -2\frac{\sum_{n=0}^{'[\Lambda/2]} (-1)^n \sum_{c\in C_n} a_c \sin(\Phi_c+\Theta/2)\,\mathrm{e}^{-n\Lambda_c/2}}{\sum_{n=0}^{'[\Lambda/2]} (-1)^n \sum_{c\in C_n} \sin(\Phi_c+\Theta/2)\,\mathrm{e}^{-n\Lambda_c/2}} \quad (28)$$

and

$$L_t^{\rm osc} = -2\frac{\sum_{n=0}^{'[\Lambda/2]} n(-1)^n \sum_{c\in C_n} \sin(\Phi_c+\Theta/2)\,\mathrm{e}^{-n\Lambda_c/2}}{\sum_{n=0}^{'[\Lambda/2]} (-1)^n \sum_{c\in C_n} \sin(\Phi_c+\Theta/2)\,\mathrm{e}^{-n\Lambda_c/2}}\,. \quad (29)$$

Note that A_t defined above is manifestly real. The form (27) can be interpreted in the following way. If one ignores the terms $A_t^{\rm osc}$ and $L_t^{\rm osc}$ one obtains the smooth or mean value for A_t which is nothing but $\frac{1}{\Lambda}\,\mathrm{tr}\,A$ which, in the semiclassical limit, approaches the ergodic average of $A = \bar{a}$. This average does not depend on the particular state $|1_t\rangle$ for which the expectation value is computed. The term $A_t^{\rm osc}$ results from the interference of many contributions from the periodic orbits and their weights a_p, and depends on the particular state considered via the composite actions and also the composite Lyapunov exponents. $L_t^{\rm osc}$ is a correction to the normalization, and as such it does not depend on the particular observable which is discussed.

We can immediately apply this result to calculate the expectation value of the scar observable $A_{\rm scar}(\theta_0)$. For this purpose, we may disregard the denominator all together, since we are only interested in the relative intensities for different values of θ_0. In the numerator we can distinguish two different sources of θ_0 dependence. The first term is proportional to $\bar{A}(\theta_0)$ and therefore it gives the smooth background. It is modulated by the

second sum, where contributions from individual composite orbits come from the factors $a_c(\theta_0)$. The resulting smooth distribution can be written as

$$p_t(\theta_0) = \bar{p}(\theta_0) + 2\frac{\sum'^{[\Lambda/2]}_{n=1}(-1)^{n+1}\sum_{c\in C_n} f_c(\theta_0)\sin(\Phi_c + \Theta/2)\ \mathrm{e}^{-n\Lambda_c/2}}{\sum'^{[\Lambda/2]}_{n=1}(-1)^{n}\sum_{c\in C_n}\sin(\Phi_c + \Theta/2)\ \mathrm{e}^{-n\Lambda_c/2}} \tag{30}$$

where $f_c(\theta_0)$ is the sum of $f(\theta_j - \theta_0)$ where j goes over the points whose union is the composite orbit c. In this way, the smooth part of the distribution is separated, and the 'oscillatory' part is expressed as a weighted average of the contributions from individual composite orbits. The weights are not positive, so that the oscillatory term results from a complicated interference. Hence the chances that the net effect is dominated by a single composite orbit are slim. This is another expression of the Shnirelman theorem, which gives a rigorous proof of the statement that *scars are scarce*! At any rate, expressions (27) and (30) have the expected form which justifies *a posteriori* the way by which we defined the representation of the wavefunctions on the section.

Before discussing some numerical results, it is worthwhile observing that the formalism presented above can be used to provide the semiclassical distribution of the eigenstates of evolution operators which describe the quantum analogues of classical mappings. As a matter of fact, the only modification necessary is to replace S by the unitary evolution operator, which now does not depend on the wavenumber k [24].

The present study can be also considered as an extension of the recent work of Eckhardt *et al* [16], who computed the semiclassical expectation values of observables in configuration space. They are expressed as weighted sums of contributions of periodic orbits. Here, we have derived a similar expression which relates to observables on the section.

3. Numerical tests

3.1. The Limacon billiard

We will apply the theory and study scars on the scattering section for the Limacon [25] billiard, whose boundary is given by

$$r(\phi) = 1 + a\cos\phi\,. \tag{31}$$

The parameter a takes values from $a = 0$ (the circle) to $a = 1$ (the Cardioid [26]). At $a = \frac{1}{2}$ the billiard has one point where the radius of curvature becomes infinite. For larger values, the Limacon is not convex and hence no infinite series of whispering gallery orbits exist, which is one of the reasons why we choose this billiard. The Cardioid has non-vanishing Lyapunov exponents [27]: however, for the values of a that give shapes between the circle and the Cardioid, no rigorous statements about the chaoticity are known. We used a value of $a = 0.6$ since we found stable periodic orbits for smaller values of a. The Limacon was first considered a billiard in [28] and since then, it was repeatedly used by various authors [26, 29].

The numerical solutions of the quantum mechanical exterior and interior problems for the Limacon are rather straightforward to get. (We shall restrict ourselves to the Dirichlet boundary conditions.) A numerically useful strategy to calculate the S-matrix is the null-field approach [30, 31] for the scattering of a billiard with Dirichlet boundary conditions. By the inside–outside duality, this also provides us with the spectrum of the billiard and the wavefunctions. In [31] the uniqueness of the solution and also the completeness of various basis sets on the boundary are demonstrated. For practical purposes, however, a simplified version for star-like billiards [11] was actually used.

Table 1.

Number of bounces	2	3	4	5	6	7	8	9	10	11	12
Number of orbits	2	2	5	4	8	10	21	28	51	79	91

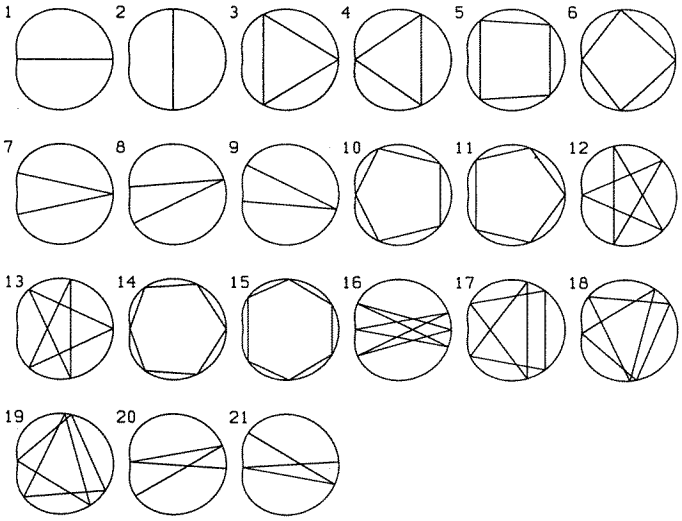

Figure 1. Primitive periodic orbits with up to six reflections from the wall.

It is much more difficult to build the necessary classical database on sufficiently long periodic orbits. The main obstacle is the lack of a symbolic code for the Limacon billiard, which is guaranteed to provide an immaculate list of periodic orbits. In table 1 we list the number of periodic orbits we found for different bounce numbers ($\leqslant 12$).

The Limacon is star-like. The Poincaré section for the classical bounce dynamics is conveniently parametrized in terms of the canonical conjugate variables θ, the direction of a chord in the billiard, and b, its impact parameter (b is related to the angular momentum by $l = kb$) [23]. To obtain an immaculate set of periodic orbits, we had to heavily oversearch the parameter space and performed various numerical tests. We are certain that we have the complete list of periodic orbits with $n \leqslant 9$ bounces, and that the number of missed periodic orbits with $9 < n \leqslant 12$ is not too large. We cannot exclude the existence of minute elliptic islands near periodic orbits which just bifurcated. The orbits with a maximum of six bounces are shown in figure 1. In addition to the number of bounces, the orbits can be classified by their winding number, a scheme that is sufficient for the circle. However, some orbits are not of the circle type. They originate from bifurcations. The first examples are the V-shaped orbits 7–9, which are bifurcates of orbit 1.

3.2. Testing the semiclassical approximation

In this section we shall make use of the classical database to construct semiclassical quantities which will be compared with the numerical quantum data. We shall check various properties which are particularly relevant to the theory developed in the preceding sections.

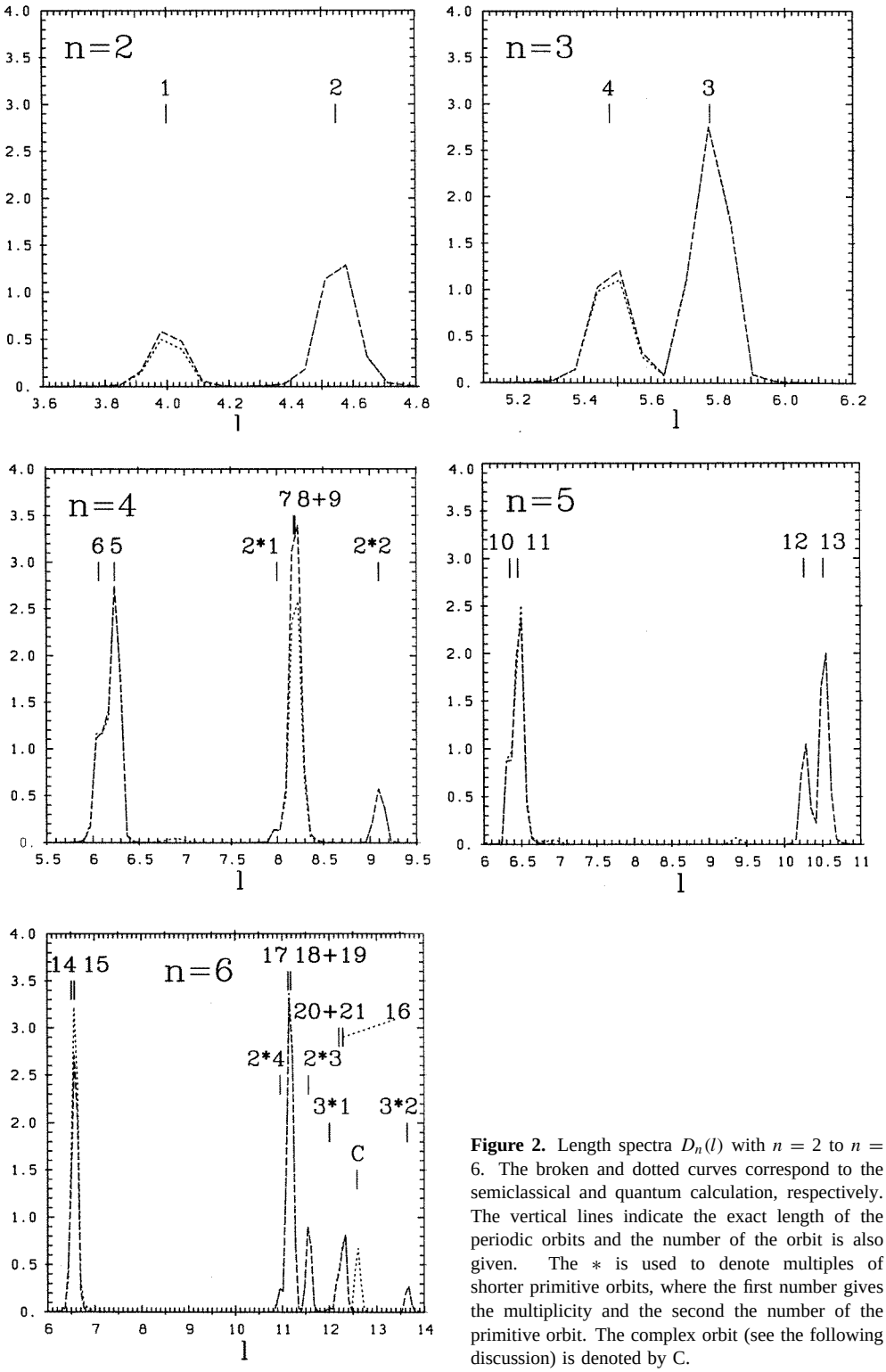

Figure 2. Length spectra $D_n(l)$ with $n = 2$ to $n = 6$. The broken and dotted curves correspond to the semiclassical and quantum calculation, respectively. The vertical lines indicate the exact length of the periodic orbits and the number of the orbit is also given. The $*$ is used to denote multiples of shorter primitive orbits, where the first number gives the multiplicity and the second the number of the primitive orbit. The complex orbit (see the following discussion) is denoted by C.

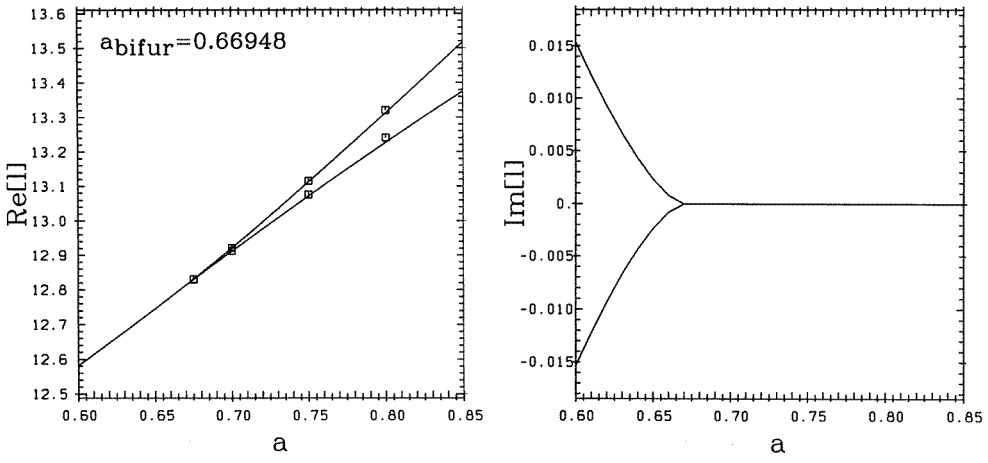

Figure 3. Creation of a new pair of orbits by bifurcation at $a_{\mathrm{bifur}} \approx 0.669\,48$. We show the real and imaginary part of the complex length calculated by expansion around the bifurcation point. The squares give the exact length of real periodic orbits and the first symbol is just after the bifurcation.

The semiclassical approximation for $\mathrm{Tr}\, S^n(k)$ is of prime importance. To check it, we compute the function

$$D_n(l) = \int_0^\infty w(k-k_0)\, \mathrm{e}^{\mathrm{i}kl}\ \mathrm{Tr}\, S^n(k)\, \mathrm{d}k \tag{32}$$

where $w(x)$ is a positive window function centred about $x = 0$. The S-matrix has been calculated and used for the Fourier transform up to $k_{\max} = 97$. $D_n(l)$ is a 'length spectrum' which selects the orbits according to their number of bounces from the boundary and is a numerically stable observable. It allows a more detailed test of the semiclassical approximation than the length spectrum obtained by a Fourier transform of the spectral density. (It follows from (1) that the latter is actually a sum over all the $D_n(l)$). The numerical and semiclassical length spectra with $n \leqslant 6$ are compared in figure 2. The agreement is generally very good. It deteriorates somewhat (see data for $n = 2$ and $n = 3$) for the orbits which bounce at the point where the curvature vanishes (i.e. orbits 1 and 4). The only significant deviation between the semiclassical length spectrum and the exact one can be seen for $n = 6$. The peak at length $l \approx 12.6$ (denoted by C in the figure) is not reproduced by the semiclassical calculation. Closer investigation reveals that a pair of new orbits is created by bifurcation at $a_{\mathrm{bifur}} \approx 0.669\,48$. For $a < a_{\mathrm{bifur}}$ this pair can be found as the complex solutions of the stationary points of the length of the periodic orbit. We calculated approximate periodic orbits by expanding around the exact solution at the bifurcation point for small changes in a. Since the Hessian matrix of the length has one zero eigenvalue at the bifurcation point it is favourable to change to a basis where the Hessian is diagonal. Then, the five equations corresponding to the non-vanishing eigenvalues can be expanded to first order, whereas the remaining equation has to be expanded to second order, since the first order vanishes. This quadratic equation yields two real solutions for $a > a_{\mathrm{bifur}}$ and two complex solutions for $a < a_{\mathrm{bifur}}$. Figure 3 shows the real and imaginary part of the complex length of the bifurcating orbits. For the real orbits we can compare our expansion with an exact determination of the periodic orbits, for the complex orbits, we can read off the real part of the length from the figure, and find agreement with the position of

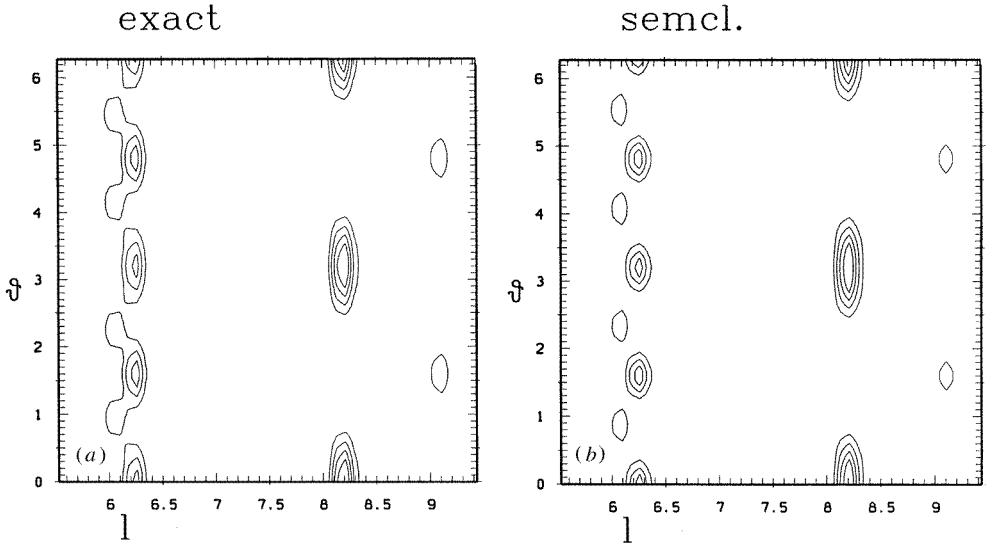

Figure 4. Length spectrum $D_4(l,\theta)$. (*a*) The exact result, (*b*) the semiclassical theory. The contour lines are equally spaced and identical in both (*a*) and (*b*).

the additional peak in figure 2. A more elaborate analysis of 'ghost orbits' can be found in [32]. Also wavefunctions scarred by 'ghosts orbits' have been observed [33]. A more relevant test of the present theory is obtained by generalizing the length spectrum (32) by replacing $\mathrm{Tr}\, S^n(k)$ by $\mathrm{Tr}\,[A_{\mathrm{scar}}(\theta)S^n(k)]$. The precise form of the observable operator (11) on the section is

$$\langle\theta'|A_{\mathrm{scar}}(\theta)|\theta''\rangle = \delta(\theta'-\theta'')\frac{1}{\sqrt{2\pi}}\frac{1}{\Delta\theta}\,\mathrm{e}^{-(\theta'-\theta)^2/2(\Delta\theta)^2}\,. \tag{33}$$

The resulting function

$$D_n(l,\theta) = \int_0^\infty w(k-k_0)\,\mathrm{e}^{\mathrm{i}kl}\,\mathrm{Tr}\left[A_{\mathrm{scar}}(\theta)S^n(k)\right]\,\mathrm{d}k \tag{34}$$

is expected to be large at points (l,θ) which correspond to lengths and angles of periodic orbits with n bounces. For each value of the length, one should observe n peaks at values of θ which mark the directions of the chords which make up the periodic orbit.

Figure 4 shows an example for $n = 4$ and the parameter $\Delta\theta = 0.2$. This angular resolution implies a numerically determined lower bound of $k_{\mathrm{min}} = 20$ and the largest k used was $k_{\mathrm{max}} = 97$. The general agreement between the semiclassical and the full numerical calculation is good and we can identify the contributions of orbits 5 and 6 at $l \approx 6.1$ and also the V-shaped orbits (7, 8 and 9) at $l \approx 8.1$. At $l \approx 9$ the repetition of one of the two bounce orbits can be seen. The repetition of orbit 1 cannot be seen at $l = 8$ both here and in figure 2 because of the large Lyapunov exponent and the neighbourhood in length to orbit 7.

Because of the rather limited number of periodic orbits at our disposal, we are not able to check (1) and (30) directly. With the present data set of orbits with $n \leqslant 12$ bounces, we would have been able to get the semiclassical ζ function in the domain $0 \leqslant k \leqslant 12$. In this domain there are 35 exact eigenvalues, out of which we were able to reproduce only the lowest three. The semiclassical theory is not expected to yield accurate eigenvalues at such low values of k.

3.3. Scarred wavefunctions

Scars are scarce, and if we want to compare them in the complete configuration space, and on the section, we have to be sure that they are really there to start with. If a wavefunction with wave number k_n is scarred by an orbit of length l, an eigenfunction with wave number $k_m \approx k_n + \frac{2\pi}{l}(m-n)$ also has a chance of being scarred by the same orbit. Here, n and m count the nodes along the trajectory [8]. To test this, we calculated all wavefunctions from $k = 10$ to $k = 52$ and visually inspected these 830 wavefunctions for scars along the simplest periodic orbits. For orbits 2 and 7 we found a set of scarred wavefunctions with 20 and 54 members, respectively. Odd and even scarred wavefunctions alternate. We confirmed that these states also appeared scarred in phase space, by computing their Husimi distributions. At small k-values a few wavefunctions also showed contributions from other periodic orbits, but this was never dominant. At high k-values, other periodic orbits had a smaller influence on the Husimi distributions of the two sets.

The node-number along the scar versus the k-value is given in figure 5 for both cases. From the slope of the curves, we can determine the length of the periodic orbits to be $l_2 = 4.541$ and $l_7 = 8.190$ whereas the exact values are $l_2 = 4.546$ and $l_7 = 8.199$. However, we could not identify a wavefunction which is scarred by orbit 7, with 29 nodes. The identification was ambiguous in three cases, where two close-by wavefunctions appeared scarred. In these cases, we used only one of them.

A similar series of scarred wavefunctions were observed by Agam and Fishman [8] for a variant of the hyperbola billiard, comprising sets for two periodic orbits with 11 and 17 scarred wavefunctions. Despite the fact that we cover a larger k-range, we cannot predict how the trend displayed in figure 5 will continue as $k \to \infty$. One clue about the large k behaviour may be given by figure 6 which shows the deviation of the k-value observed to the fitted line in units of the mean spacing between two wavefunctions. We recognize a relatively large fluctuation around the mean. We can interpret this with the help of (30). To create a scar, it is not sufficient that a single term in the sum is large, but also, all other terms have to interfere destructively. Thus, there is a window around each maximum of a particular term in (30) for which the wavefunctions are candidates to be scarred. But all other terms determine whether a scar can really be observed. As k increases, the number

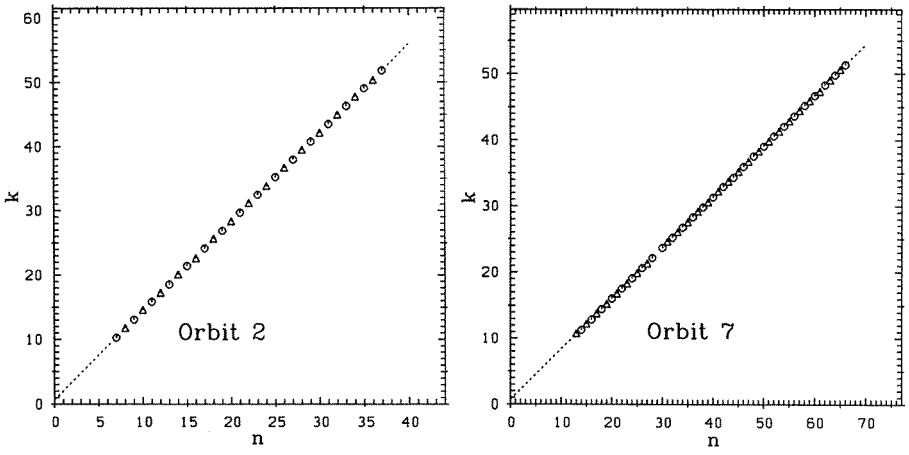

Figure 5. The k-values of the wavefunctions scarred by orbit 2 and 7. The circles correspond to odd wavefunctions, the triangles to even ones.

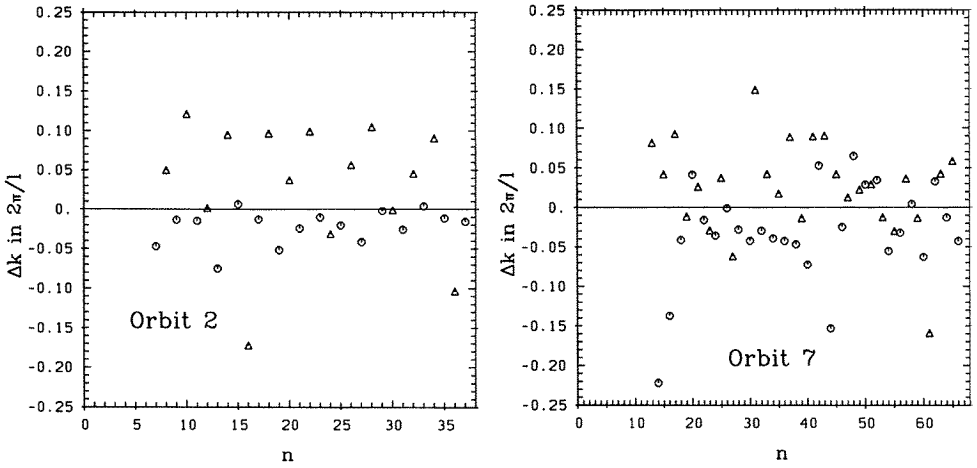

Figure 6. The same as the previous figure, but deviation from linear behaviour for orbits 2 and 7.

of periodic orbits contributing to the sum increases exponentially. On the other hand, for a fixed window size, the number of candidates for scarred wavefunctions increases only linearly. How these two effects will balance is not clear *a priori*.

We also have to add that we could not find a set of scarred states even in cases where they should be easy to observe because of a small Lyapunov exponent. In particular, we could not find a set for one of the triangular orbits. This is due to the existence of some orbits with nearly the same length, which make the interference very complicated and may induce some beat phenomena.

We shall now show how the scars which we have unambiguously established in configuration space appear on the scattering section as predicted in (30).

The representation of the eigenfunction on the section is the eigenvector of the S-matrix with eigenvalue 1. Its components in the angular momentum basis are s_l^t so that

$$\langle\theta|1_t\rangle = \sum_{l=-\Lambda/2}^{\Lambda/2} s_l^t \, \mathrm{e}^{\mathrm{i}l\theta} \, . \tag{35}$$

Thus for the observable, we obtain

$$\langle 1_t|A_{\mathrm{scar}}(\theta_0)|1_t\rangle \approx \sum_{l,n=-\Lambda/2}^{\Lambda/2} s_l^{t\,*} s_n^t \, \mathrm{e}^{-\frac{1}{2}(l-n)^2\Delta\theta^2} \, \mathrm{e}^{\mathrm{i}(l-n)\theta_0} \, . \tag{36}$$

This eigenvector s_l^t also determines the wavefunction

$$\langle \boldsymbol{r}|1_t\rangle = \sum_{l=-\Lambda/2}^{\Lambda/2} s_l^t \, J_l(kr)\mathrm{i}^l \, \mathrm{e}^{\mathrm{i}l\theta} \tag{37}$$

in the coordinate representation. In the numerical calculation of the wavefunctions, Λ is taken larger than its semiclassical value to ensure the unitarity of the S-matrix and the precision of the calculation. Without any exception, these wavefunctions agree inside the billiard with the eigenfunctions determined using the collocation method [34].

In figures 7 and 8 we present two examples for both, orbits 2 and 7, that nicely demonstrate the scars on the section. In the cases of orbit 7, a smaller value $\Delta\theta = 0.05$

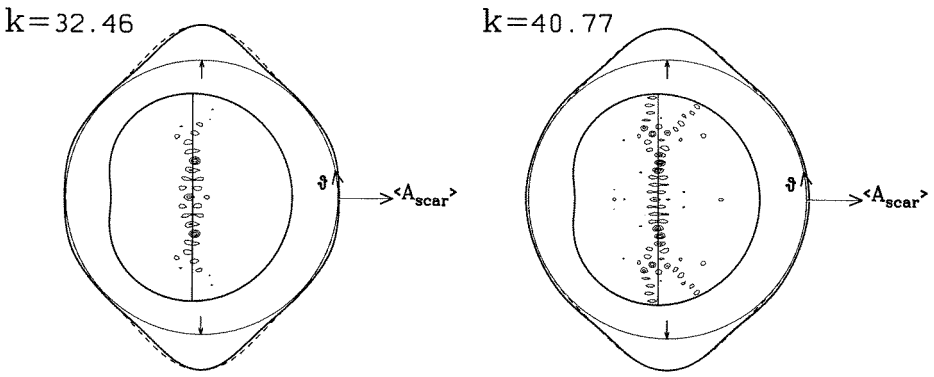

Figure 7. Two examples for scars in configuration space and on the scattering section for orbit 2. The line inside the billiard gives the periodic orbit. The outermost bold line gives the expectation value of $A_{\rm scar}(\theta)$, where the reference line of zero intensity is given by the inscribed circle. The arrows indicate the directions (values of θ) corresponding to the periodic orbit and the broken line the semiclassical curve for this orbit.

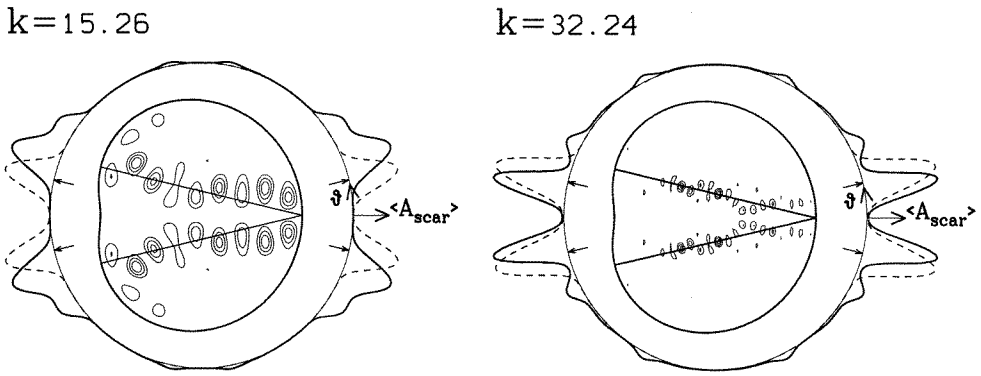

Figure 8. Like previous figures but for orbit 7.

was used to obtain narrower peaks. For orbit 2 the observable (36) has only two peaks at $\pi/2$ and $-\pi/2$ but for orbit 7 additional peaks can be seen and the dominant peaks are also shifted. But also in the coordinate representation, a pure scar can never be observed. In particular close to the boundary, the scars are strongly deteriorated from an ideal shape and also modified by the presence of other orbits. In the same way scars on the section might be modified due to interference from other orbits.

Finally, we will define the section Wigner function by

$$\begin{aligned} f_{\rm W}(L,\theta) &= \int_0^{2\pi} \left\langle \theta + \frac{\phi}{2} \middle| 1_t \right\rangle \left\langle 1_t | \theta - \frac{\phi}{2} \right\rangle {\rm d}\phi \\ &= 2\pi \sum_l s_{L+\frac{l}{2}} s^*_{L-\frac{l}{2}} \, {\rm e}^{{\rm i}\theta l} \end{aligned} \tag{38}$$

and the corresponding Husimi function

$$f_{\rm H}(l_0,\theta_0) = \int\int {\rm e}^{-\frac{(l-l_0)^2}{2\Delta l^2} - \frac{\Delta l^2(\theta-\theta_0)^2}{2}} f_{\rm W}(l,\theta)\, {\rm d}l\, {\rm d}\theta \tag{39}$$

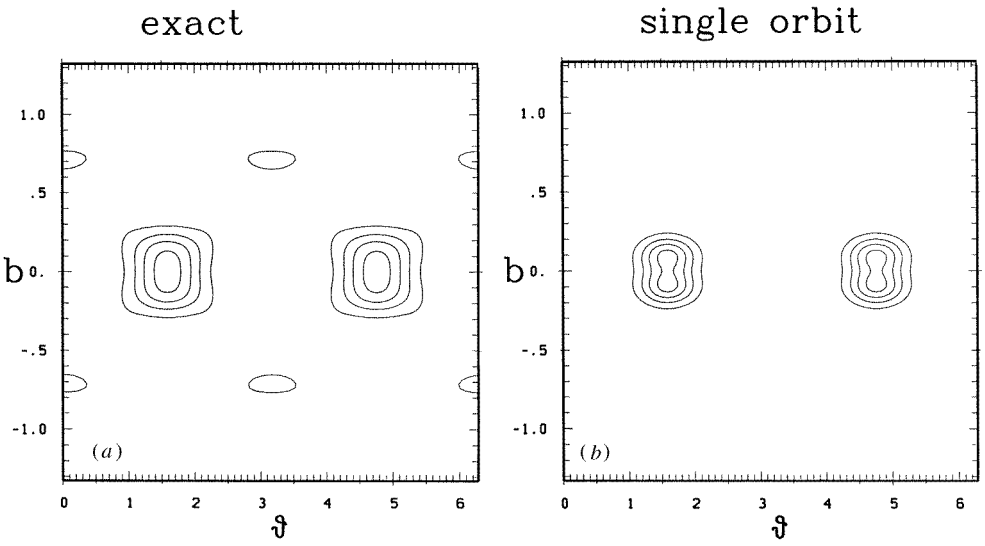

Figure 9. Husimi distribution for the eigenstate at $k = 40.77$, which is scarred by orbit 2. (a) Shows the exact result and (b) the semiclassical prediction for a state scarred only by orbit 2.

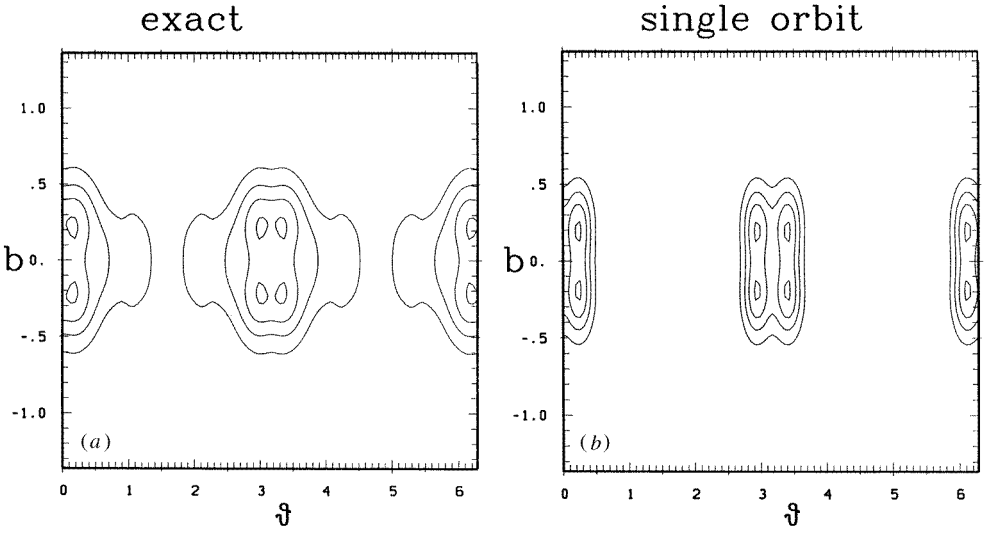

Figure 10. As for the previous figure, but for a state scarred by orbit 7 at $k = 35.26$.

which gives us the opportunity to look not only at the angular distribution but to determine the angle and angular momentum for each chord of the periodic orbit. The observable operator A is the projection on a coherent state in the angular momentum representation and the formalism as presented in the second section applies.

In figures 9 and 10 we display the exact numerical results (figures 9(a) and 10(a)) and the picture that is expected if the state is scarred only by one orbit (figures 9(b) and 10(b)), for a state scarred by orbit 2 (figure 9) and the state scarred by orbit 7 (figure 10). In the figure we changed from angular momentum to impact parameter b. Orbit 2 does

not pass exactly through the origin and hence the semiclassical picture shows peaks at non-vanishing b which are hard to resolve in the exact calculation, but can be guessed because of the elongation of the peak in the b-direction. For orbit 7 the picture is much clearer, because of the larger impact parameter, and all peaks can be clearly identified in both pictures. In all cases, the structures in the exact calculation are smoothed out, but hardly any additional peaks due to other periodic orbits appear.

4. Discussion

In the preceding sections we developed the semiclassical theory for the computation of smooth observables on Poincaré sections. We used the scattering approach to construct the Hilbert space which represents the phase space of the section, and to identify the proper representation of the complete wavefunction in this space. The semiclassical theory resulted in an expression which provides the expectation value of the observable operator as a weighted sum of contributions from periodic orbits. The formalism was then illustrated for the study of scars on a Poincaré section which is used to quantize the Limacon billiard within the scattering approach.

There are many methods by which one can define the Poincaré section, and even the scattering approach offers a few variants. In the present study we concentrated on the quantization of billiards using the exterior–interior duality [11, 20]. The Poincaré section in this case is the domain in the (l, θ) plane. An alternative quantization scheme can be achieved by connecting the system to a channel and in this way defining the auxiliary scattering system [10, 13, 14]. Here, the position on the interface and the component of the momentum parallel to it provide the classical Poincaré section. The corresponding Hilbert space is spanned by the transversal eigenfunctions which correspond to conducting modes in the channel. The formalism which we developed can be easily extended to the channel construction.

In the scattering approach, we locate an eigenenergy E_t by requiring that a certain eigenvalue of the $S(E)$ matrix approaches 1 as E approaches E_t. Truncating the Hilbert space to include a finite number of evanescent waves, the corresponding eigenvector $|1_t\rangle$ exists, and is identified as the appropriate representation of the system wavefunction on the section Hilbert space. This construction can be explained in the following way. The scattering approach is based on the idea that a unit eigenvalue of the truncated scattering matrix implies that there exists a linear combination of incoming waves which go through the scattering system as if the latter is approximately transparent [21]. In other words, the exterior wavefunction described by this linear combination can be extended into the interior. The coefficients of this linear combination are determined by the eigenvector $|1_t\rangle$. At this point it is convenient to specialize the discussion, and we shall consider the approach based on scattering in the plane. In this case, the wavefunction which satisfies the boundary conditions, and is regular both in the interior and the exterior, is given by (37). Writing the Bessel functions as a sum of incoming and outgoing cylindrical waves, and using the asymptotic expressions of the Hankel functions, we can calculate the incoming current density

$$J(\theta) = \frac{1}{2\pi} \left| \sum_{l=-\Lambda/2}^{\Lambda/2} s_l \, \mathrm{e}^{\mathrm{i}l\theta} \right|^2 . \tag{40}$$

Thus, the quantity which we computed semiclassically (after some smoothing) is the current density. A similar interpretation can be given to the section wavefunction when the channel

approach is used for quantization.

One of the important lessons we have learned from the present work is how difficult it is to identify scars and how much care one has to exercise in their study. The periodicity of scars may, for example, help us to interpret the results in [35], where the authors noted, that 'to our surprise, we found only one brilliant example of an intense scar'. In that work, 19 even-parity states around the 2000th even-parity state have been investigated and one state was scarred by orbit 2. In [36] no obvious scars have been observed to the authors' astonishment, but only eight states around the 200 000th state were scrutinized. However, using the density of states, we can easily observe, that it might be necessary to calculate 96 wavefunctions in the first case and 670 for the second case in order to have a good chance to observe one wavefunction scarred by orbit 2. This is another numerical example that almost all states are non-scarred [1]. Note that also for Hamiltonian systems, such a series of scarred states can be identified. In [17] a large number of wavefunctions of the quartic oscillator are calculated and displayed. From the figures therein, it is easy to identify for one periodic orbit a set with 19 members and the correct periodicity. Thus, the study of series of scars may help to elucidate the origin of scars by superposition of contributions from periodic orbits.

Acknowledgments

We would like to thank the Minerva Center for Nonlinear Physics and DK would also like to thank the Minerva Foundation for financial support. H Primack and I Ussishkin have always been enthusiastic about discussing all the problems that occured while this work was being performed, which we enjoyed and appreciated very much.

References

[1] Shnirelman A I 1974 *Usp. Mat. Nauk.* **29** 181
[2] McDonald S W 1983 *PhD Thesis* Lawrence Berkeley Laboratory LBL 14837
[3] Heller E J 1984 *Phys. Rev. Lett.* **53** 1515
[4] Bogomolny E B 1988 *Physica* **31D** 169
[5] Berry M 1989 *Proc. R. Soc.* A **423** 219
[6] Agam O and Fishman S 1993 *J. Phys. A: Math. Gen.* **26** 2113
[7] Berry M V and Keating J P 1992 *Proc. R. Soc.* A **437** 151
[8] Agam O and Fishman S 1994 *Phys. Rev. Lett.* **73** 806
[9] Bogomolny E B 1992 *Nonlinearity* **5** 805
[10] Doron E and Smilansky U 1992 *Nonlinearity* **5** 1055
[11] Dietz B and Smilansky U 1993 *Chaos* **3** 581
[12] Gutzwiller M C 1971 *J. Math. Phys.* **12** 343
[13] Schanz H and Smilansky U 1995 *Chaos, Solitons and Fractals* **5** 1289
[14] Rouvinez C and Smilansky U 1995 *J. Phys. A: Math. Gen.* **28** 77
[15] Prosen T 1994 *J. Phys. A: Math. Gen.* **27** L709
[16] Eckhardt B, Fishman S, Müller K and Wintgen D 1992 *Phys. Rev.* A **45** 3531
[17] Eckhardt B, Hose G and Pollak E 1989 *Phys. Rev.* A **39** 3776
[18] Smilansky U 1992 *Chaos and Quantumchaos* ed W D Heiss p 57
[19] Jung C 1986 *J. Phys. A: Math. Gen.* **19** 1345
[20] Eckmann J-P and Pillet C-A 1995 *Commun. Math. Phys.* **170** 283
[21] Dietz B, Eckmann J-P, Pillet C-A, Smilansky U and Ussishkin I 1995 *Phys. Rev.* E **51** 4222
[22] Artuso R, Aurell E and Cvitanovic 1990 *Nonlinearity* **3** 325
[23] Smilansky U 1995 *Proc. 1994 Les Houches Summer School on 'Mesoscopic Quantum Physics'* ed E Akkermans
[24] Agam O and Brenner N 1994 Semiclassical Wigner functions of quantum maps on a torus *Preprint* TECHNION-PHY-94

[25] 1978 *Dictionary of Physics and Mathematics* (New York: McGraw-Hill)
[26] Bäcker A, Steiner F and Stifter P 1994 Spectral statistics in the quantized cardioid billiard *Desy-Preprint* DESY 94-213
[27] Wojtkowski M 1986 *Commun. Math. Phys.* **105** 391
[28] Robnik M 1983 *J. Phys. A: Math. Gen.* **16** 3971
[29] Mehlig B, Boosé D and Müller K 1995 *Phys. Rev. Lett.* **75** 57
[30] Waterman P C 1965 *Proc. IEEE* **53** 805
[31] Martin P A 1982 *Wave Motion* 391
[32] Kuś M, Haake F and Delande D 1993 *Phys. Rev. Lett.* **71** 2167
[33] Bellomo P and Uzer T 1995 *Phys. Rev.* A **51** 1669
[34] Kuttler J R and Sigillito V G 1984 *SIAM Rev.* **26** 163
[35] Prosen T and Robnik M 1993 *J. Phys. A: Math. Gen.* **26** 5365
[36] Li B and Robnik M 1994 *J. Phys. A: Math. Gen.* **27** 5509